

Quantal and classical differential-scattering calculations for the electron-impact excitation of argon ions

M. S. Pindzola

Department of Physics, Auburn University, Auburn, Alabama 36849

D. R. Schultz

Physics Division, Oak Ridge National Laboratory, Oak Ridge, Tennessee 37831

D. C. Griffin

Department of Physics, Rollins College, Winter Park, Florida 32789

(Received 11 June 1993)

Electron-scattering cross sections for the $3s \rightarrow 3p$ dipole transition in Ar^{7+} are calculated in both the quantal distorted-wave approximation and the classical-trajectory Monte Carlo method. The two approaches are in substantial agreement for the angular differential cross section at 20-, 50-, and 100-eV incident electron energy. This result indicates the degree to which classical scattering influences the dipole excitation. Further distorted-wave calculations are made for the $3s \rightarrow 3d$ and $3s \rightarrow 4s$ transitions in Ar^{7+} and the $3s^2\ ^1S \rightarrow 3s3p\ ^3,^1P$ transitions in Ar^{6+} . The forward-backward asymmetry in the angular distribution of scattered electrons is examined for each transition. All transitions exhibit strong backward scattering at energies near the excitation threshold.

PACS number(s): 34.80.Kw

I. INTRODUCTION

The angular differential cross section for an electron scattering process is generally a stronger probe of the details of the collision dynamics than the integrated total cross section. For low energies, where a partial-wave quantal analysis is appropriate, the differential cross section measures both the magnitude of and the relative phase between the scattering matrix elements. The recent development of crossed-beams experiments [1], to measure fixed-angle differential cross sections, and merged-beams experiments [2,3], to measure partial cross sections integrated over a range of angles, gives added incentive to an examination of the differential scattering dynamics found in electron collisions with multiply charged ions.

In this paper we employ the perturbative distorted-wave method [4] to examine the quantal aspects of the differential cross section for the electron excitation of both Ar^{6+} and Ar^{7+} . For these ions the distorted-wave method should provide accurate nonresonant cross sections, since the method generally yields more exact cross sections as the residual target-ion charge increases [5,6]. Of special interest to the design of the merged-beams experiments is the strength of the backward scattering as a function of transition type and incident electron energy. To delineate the classical aspects of the differential cross sections, we employ the classical-trajectory Monte Carlo method [7] to calculate the $3s \rightarrow 3p$ excitation of Ar^{7+} . A direct comparison of the quantal and classical calculations reveals the underlying dynamics common to both, as well as the limitations of the classical approach (or more precisely, the statistical quasiclassical approach).

In the following paragraphs we first present summaries of the quantal distorted-wave method in Sec. II and the

classical trajectory Monte Carlo method in Sec. III. In Sec. IV the quantal and classical methods are compared for the differential cross section for the $3s \rightarrow 3p$ dipole transition in Ar^{7+} . In Sec. V the forward-backward asymmetries for the $3s \rightarrow 3p$, $3d$, $4s$ transitions in Ar^{7+} and the $3s^2\ ^1S \rightarrow 3s3p\ ^3,^1P$ transitions in Ar^{6+} are presented. Finally, in Sec. VI, we provide a brief summary of the results.

II. QUANTAL DISTORTED-WAVE THEORY

The fully quantal close-coupling method for the calculation of electron-ion excitation cross sections is based on a partial-wave expansion of the total wave function for the $(N+1)$ -electron system in terms of a previously calculated spectrum of N -electron target-ion states [4]. The close-coupling equations for the continuum radial wave functions $F_{ij}(r)$ are given by (in atomic units)

$$\left[-\frac{1}{2} \frac{d^2}{dr^2} + \frac{l_i(l_i+1)}{2r^2} - \frac{Z}{r} + V_{ii} - \frac{k_i^2}{2} \right] F_{ii}(r) + \sum_{j \neq i} V_{ij} F_{ji}(r) = 0. \quad (1)$$

The channel index i denotes a collection of quantum numbers $(L_i S_i k_i l_i \mathcal{L} \mathcal{S} \Pi)$ which couple the orbital (L_i) and spin (S_i) angular momentum of the target ion with the orbital (l_i) and spin angular momentum of the scattered electron to yield the total orbital (\mathcal{L}) and spin (\mathcal{S}) angular momentum of the $(N+1)$ -electron system. The second index i' represents the index of the incident channel, while k_i is the linear momentum of the scattered electron. The potential operators V_{ij} contain direct and exchange electrostatic terms; as well as exchange-overlap

terms, which arise because of the nonzero overlap between bound and continuum orbitals with the same orbital angular momentum.

For multiply charged atomic ions, the close-coupling equations of Eq. (1) may be accurately solved for the non-resonant excitation cross section in the unitarized distorted-wave approximation [6]. We drop all potential terms V_{ij} (with $i \neq j$), in Eq. (1), which couple the various channels, and solve the differential equations

$$\left[-\frac{1}{2} \frac{d^2}{dr^2} + \frac{l_i(l_i+1)}{2r^2} - \frac{Z}{r} + V_{ii} - \frac{k_i^2}{2} \right] f_i(r) = 0, \quad (2)$$

where the asymptotic form of the radial distorted-wave function $f_i(r)$ is one times a sine function. The angular differential cross section for excitation from an initial term $L_i S_i$ to a final term $L_f S_f$ is given by [8]

$$\begin{aligned} \frac{d\sigma_{if}}{d\Omega} = & \frac{1}{8(2L_i+1)(2S_i+1)k_i^2} \\ & \times \sum_{\lambda} (2\lambda+1) \left[\sum_{l_i, l_f} \sum_{l'_i, l'_f} \begin{Bmatrix} l_i & l'_i & \lambda \\ 0 & 0 & 0 \end{Bmatrix} \begin{Bmatrix} l_f & l'_f & \lambda \\ 0 & 0 & 0 \end{Bmatrix} i^{(l_i-l_f)(l'_i-l'_f)} e^{i(\sigma_{l_i}-\sigma_{l'_i}+\sigma_{l_f}-\sigma_{l'_f})} \right. \\ & \times \sum_{j_t} (-1)^{j_t+\lambda} (2j_t+1) \begin{Bmatrix} l_i & l_f & j_t \\ l'_i & l'_f & \lambda \end{Bmatrix} \\ & \left. \times \sum_{\mathcal{S}} M^*(L_i S_i l'_i L_f S_f l'_f j_t \mathcal{S}) M(L_i S_i l_i L_f S_f l_f j_t \mathcal{S}) \right] P_{\lambda}(\cos\theta). \quad (3) \end{aligned}$$

The sums in Eq. (3) are performed over the multipolar-expansion parameter λ , the free-electron angular momenta l , the momentum-transfer quantum number j_t , and the total spin angular momentum \mathcal{S} . The function M is defined by the equation

$$\begin{aligned} M(L_i S_i l_i L_f S_f l_f j_t \mathcal{S}) = & \sum_{\Pi, \mathcal{L}} (-1)^{l_i+l_f} \sqrt{(2l_i+1)(2l_f+1)(2\mathcal{S}+1)} \\ & \times (-1)^{\mathcal{L}} (2\mathcal{L}+1) \begin{Bmatrix} L_i & L_f & j_t \\ l_f & l_i & \mathcal{L} \end{Bmatrix} T(L_i S_i l_i \rightarrow L_f S_f l_f; \mathcal{L} \mathcal{S} \Pi). \quad (4) \end{aligned}$$

In the distorted-wave approximation the off-diagonal elements of the ρ matrix are given by

$$\rho_{fi} = \frac{-2}{\sqrt{k_i k_f}} \int_0^{\infty} f_f(r) V_{fi} f_i(r) dr, \quad (5)$$

and the diagonal elements of the ρ matrix are zero. The reactance matrix R is found by the transformation

$$R = (\sin\delta + \cos\delta\rho)(\cos\delta - \sin\delta\rho)^{-1}, \quad (6)$$

where δ is a diagonal matrix containing the non-Coulomb phase shifts δ_i . The transition matrix T , whose elements are found in Eq. (4), is related to the reactance matrix R by the equation

$$T = \frac{-2iR}{(1-iR)}. \quad (7)$$

For Ar^{6+} and Ar^{7+} the bound-state orbitals were generated in the single-configuration Hartree-Fock approximation [9] and then used to construct the potentials V_{ij} found in Eqs. (2) and (5). Experimental energies [10] were used for the LS term separations in both Ar^{6+} and Ar^{7+} . The partial-wave expansion for the differential cross section of Eq. (3) included all values up to $\mathcal{L} = 50$.

III. CLASSICAL-TRAJECTORY MONTE CARLO THEORY

A large number of works have established the utility of the classical-trajectory Monte Carlo technique in describing the intermediate-energy collisions of ions with atoms. Comparatively fewer studies have explored its application to light-particle impact; however, several recent studies have examined in detail singly and doubly differential cross sections for ionization by electron and positron impact [11–13]. The classical-trajectory Monte Carlo method was first applied to atomic collisions by Abrines and Percival [7], adapting Monte Carlo methods previously employed in the study of molecular collisions. In brief, the technique is the simulation of a collision in which a large ensemble of initial electronic configurations is sampled in order to reproduce as well as possible the quantum-mechanical position and momentum distributions, and therefore the wave function, of the ion or atom. The subsequent motion of the projectile, target electron(s) and target core are then followed by solving the classical Hamiltonian equations for a sequence of time steps through the collision. Once the particles have separated, knowledge of their positions and momenta allows one to compute the scattering angle of any free electrons, and the binding energies and orbital angular mo-

menta of any bound electrons. Several specific variations of the general model are described below pertinent to the present application to electron-impact excitation of Ar^{7+} .

To begin with, since the target contains a single electron outside closed shells, we represent it by a single active electron bound by an amount given by the experimental ionization potential of 143.5 eV [10]. The interaction of this electron with the core, as well as that of the projectile electron, is represented by a parametrized Hartree-Fock model potential [14]. In addition, since the target electron initially occupies the $3s$ state, we reject from the initial conditions generated through the usual Monte Carlo sampling any orbits which do not correspond to $n=3$ and $l=0$. The quantal n and l corresponding to the classical values obtained are specified by the procedure described by Becker and MacKellar [15] in which the classical n level is given by

$$n_c = Z_e / (2U)^{1/2}, \quad (8)$$

where Z is the effective nuclear charge and U is the binding energy in atomic units, and the classical l level is given by

$$l_c = [(xy - y\dot{x})^2 + (xz - z\dot{x})^2 + (yz - z\dot{y})^2]^{1/2}, \quad (9)$$

where x , y , and z are the Cartesian coordinates of the electron relative to the nucleus. The corresponding quantal n and l are found by determining if the classical values lie within the ranges specified by

$$[(n-1)(n-\frac{1}{2})n]^{1/3} \leq n_c \leq [n(n+\frac{1}{2})(n+1)]^{1/3} \quad (10)$$

and

$$l \leq \frac{n}{n_c} l_c \leq l+1. \quad (11)$$

The effective nuclear charge Z_e has been chosen so as to provide a convenient correspondence of the classical n levels to the quantum n levels. For example, if we were to use $Z_e=8$, corresponding to the charge the valence electron would experience if removed to a large distance from the remaining ion (Ar^{8+}), the $3s$, $3p$, and $3d$ levels would have classical n values of 2.46, 2.63, and 2.92, respectively, using the spectroscopic energy levels compiled by Kelly [10]. If instead we chose $Z_e=9$, indicating that the core levels less than completely screen the unbalanced charge, these classical n levels are 2.77, 2.96, and 3.28. This procedure amounts to the choice of a quantum defect. Thus, the initial state is chosen so that it has the correct experimental binding energy and classical values of n and l which correspond to the $3s$ state.

After the initial conditions have been set and a randomly selected impact parameter is chosen for the projectile electron, the classical path of each particle is followed until the projectile or the target electron has escaped into the asymptotic regime. This procedure is repeated for a large number of projectile-target configurations (e.g., 250 000 to 750 000 events) and on each trial, the final state is examined to determine if $3s$ and $3p$ excitation has occurred. In this case the scattering angle of the free

electron is recorded and ultimately the differential cross section may be determined. Since in this model based on classical dynamics, a range of energy losses of the projectile can cause $3s \rightarrow 3p$ excitation, in contrast to the quantal requirement of 17.6 eV, we must choose an appropriate subset. Inspection of Fig. 1, in which we compare the spectroscopic energy levels with the corresponding classical n levels computed as above, suggests that a small interval in classical n (denoted Δ in the figure), lying between the $3s$ and $3p$ levels should be assigned to represent the $3p$ state. By choosing a range of values for this parameter and comparing to the distorted-wave calculations, we have chosen a range of ± 12.5 eV. The results were not very sensitive to choices ranging from 7.5 to 15 eV. In the absence of a more robust theory of the correspondence of classical and quantal levels in ions of this complexity, this choice satisfies the criteria that the final state should have $n=3$ [using Eq. (10) with $Z_e=9$], $l=1$, and that an energy loss, centered about the quantal value of 17.6 eV, should have taken place. The range chosen may be considered an adjustable parameter of the final level binning, being fixed by comparison with the distorted-wave calculations and being not very sensitive to changes in its magnitude.

Finally, we note that electron exchange is included in the classical calculations in that whenever as a result of the collision the projectile electron remains bound to the target core and the target electron is free, classical exchange has occurred. We have found that for the transition described here, classical exchange is entirely negligible.

IV. DIFFERENTIAL CROSS SECTIONS FOR Ar^{7+}

Quantal and classical scattering calculations for the electron-impact excitation of the $3s \rightarrow 3p$ dipole transition in Ar^{7+} are presented in Figs. 2–4. The cross sections

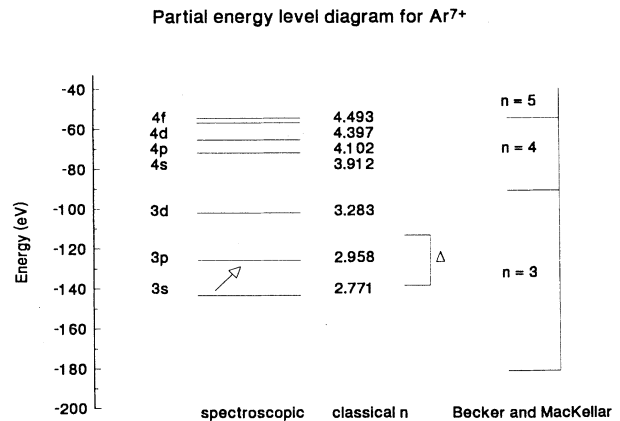


FIG. 1. Partial energy-level diagram for Ar^{7+} comparing the spectroscopic energy levels belonging to the $n=3$ and 4 manifolds [10] with the corresponding classical n levels and the established classical binning scheme of Becker and MacKellar [15]. The energy range (or classical n -level interval) denoted by Δ indicates our choice of a binning for the $3p$ state and an effective nuclear charge of $Z_e=9$ was utilized (see text).

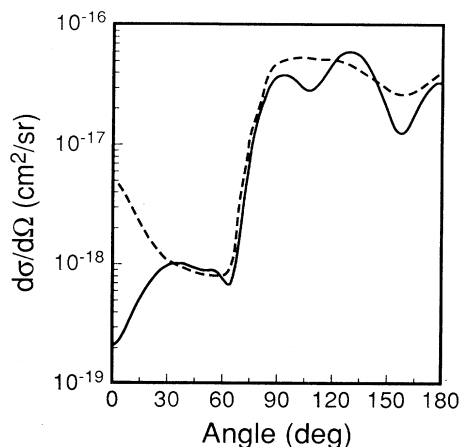


FIG. 2. The differential cross section for the $3s \rightarrow 3p$ excitation of Ar^{7+} at 20-eV incident electron energy. Solid curve, quantal distorted-wave method; dashed curve, classical-trajectory Monte Carlo method.

are differential in angle at incident energies of 20, 50, and 100 eV; where the threshold for excitation is 17.6 eV. The distorted-wave calculations for Ar^{7+} at 20 eV are in good agreement with previous close-coupling calculations [16] for $\theta > 30^\circ$. At the two higher energies, the distorted-wave results are found to be in excellent agreement with other similar calculations [1,17]. A smooth curve has been drawn through the center of the limits of the statistical uncertainties of the classical-trajectory Monte Carlo results. Typical one standard deviations were less than 5%. When compared with the distorted-wave results, the classical-trajectory Monte Carlo calculations reveal that the dominant mechanisms in action in the $3s \rightarrow 3p$ excitation are classical in origin, while the distorted-wave approach indicates that the classical scattering is modified by quantum superposition. For example, as has been illustrated in many contexts, when a

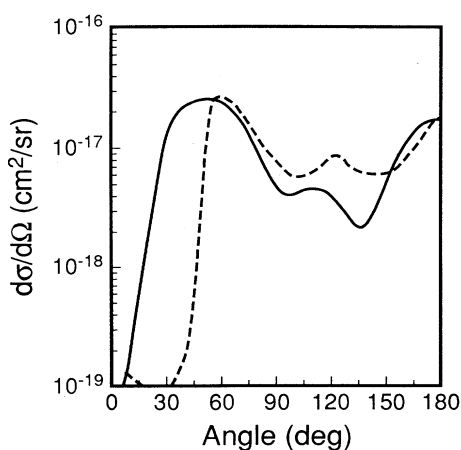


FIG. 3. The differential cross section for the $3s \rightarrow 3p$ excitation of Ar^{7+} at 50-eV incident electron energy. Solid curve, quantal distorted-wave method; dashed curve, classical-trajectory Monte Carlo method.

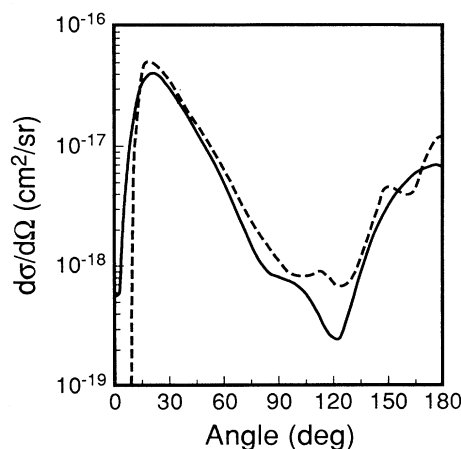


FIG. 4. The differential cross section for the $3s \rightarrow 3p$ excitation of Ar^{7+} at 100-eV incident electron energy. Solid curve, quantal distorted-wave method; dashed curve, classical-trajectory Monte Carlo method.

relatively low-energy electron scatters from a screened nucleus, an enhancement of backward scattering is observed over that from a pure Coulomb potential. (See, for example, Ref. [18] for consequences of this effect in ion-atom collisions and figures comparing the elastic scattering of electrons from either screened potentials or the Coulomb potential). In the present case, since the projectile must pass relatively close to the ion to induce excitation, it may experience a rapidly changing effective charge. This has the effect that the electron is accelerated from its initial Coulomb trajectory in the presence of the asymptotic ionic charge, and backward scattering is enhanced. Also, since relatively few partial waves contribute significantly, the differential cross section shows oscillations analogous to diffractive scattering. This diffraction also occurs classically, but, as evidenced by comparison of the classical-trajectory Monte Carlo and quantal distorted-wave results, it does not correspond identically with quantal scattering. We note that the enhancement in the backward direction shown by the distorted-wave approach over a Coulomb-Born treatment has been illustrated by Huber *et al.* [1] and Hervieux and Guet [19].

Several specific comments regarding the comparison of the classical-trajectory Monte Carlo and distorted-wave results also seem appropriate. For example, for 20-eV electron impact (Fig. 2), the classical-trajectory Monte Carlo result picks up very precisely the rapid rise of the cross section near 60° , and then plateaus at a level very much consistent with the distorted-wave result. In this backward-scattering regime, we see evidence of the diffractive scattering both in the quantal and classical cases. The rise of the classical trajectory Monte Carlo result at small angles is attributed to the fact that the energy-loss criteria employed is not sufficient for all scattering angles and a remnant of the elastic-scattering channel is being picked up. It is, in fact, the elastic channel which is intimately related to the very small cross section at small angles. From the classical analysis it is seen

that large-impact-parameter collisions, and therefore those contributing to small scattering angles, are predominantly elastic events, since it requires some significant momentum and energy transfer to cause the excitation. Thus, those events in which excitation occurs are characterized by scattering through some relatively large angle. The semiclassical model of Hervieux and Guet [19] predicts well how the peak created by this mechanism shifts to smaller angles with increasing energy. Quite simply, for higher impact energies, a smaller relative transfer of energy is necessary to cause the transition, and the electron need not be deflected as much.

Agreement with the distorted-wave results is not as good regarding the initial rise of the cross section with increasing scattering angle for 50-eV electron impact (Fig. 3), but the plateau and its variation is well reproduced. Finally, for 100-eV electron impact (Fig. 4), both the rise and the fall of the cross section through the maximum and the backward enhancement are very well reproduced by the classical-trajectory Monte Carlo model. Thus, our conclusion is that the dominant scattering mechanisms present in this excitation are classical in origin, but quantal corrections due to the fact that the diffractive scattering arises from the contributions of relatively few partial waves give rise to important modifications. Also, as observed by Reinhold and Burgdorfer [20] who compared classical and quantal treatments of ionization, the breakdown of the classical-quantal scattering correspondence is great for small-momentum-transfer, large-impact-parameter collisions. This is evident in the excitation cross section at 20 eV where such collisions dominate at small angles, leading to the discrepancy noted above. However, for higher impact energies, where smaller-impact-parameter ranges are active and the momentum transfers generally greater, the classical small-angle behavior is more like that exhibited by the quantal results.

For completeness, total cross sections for the electron-impact excitation of the $3s \rightarrow 3p$ dipole transition in Ar^{7+} are presented in Table I. As is well known [21], the classical model yields total cross sections in the high-energy limit which vary in proportion to $1/E$ for a given energy E , for dipole-allowed excitation or for ionization. In contrast, quantum-mechanical results decrease as some constant times $\ln(E)/E$.

V. FORWARD-BACKWARD ASYMMETRIES FOR Ar^{7+} AND Ar^{6+}

Quantal distorted-wave calculations for the electron-impact excitation of the $3s \rightarrow 3p$, $3d$ and $4s$ transitions in

TABLE I. Total cross sections for the electron-impact excitation of the $3s \rightarrow 3p$ transition in Ar^{7+} .

Energy (eV)	Quantal distorted wave (10^{-18} cm^2)	Classical-trajectory Monte Carlo (10^{-18} cm^2)
20	267	405
50	122	115
100	71	105

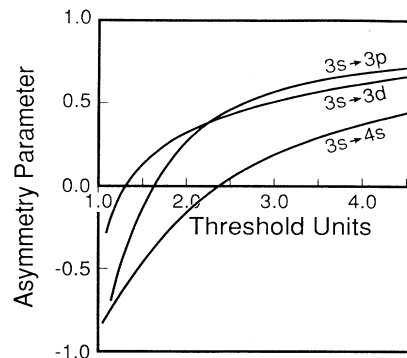


FIG. 5. The forward-backward asymmetry parameter for the $3s \rightarrow 3p$, $3s \rightarrow 3d$, and $3s \rightarrow 4s$ excitations in Ar^{7+} . (Threshold unit is the incident energy divided by the excitation energy.)

Ar^{7+} and the $3s^2 1S \rightarrow 3s3p^1 3P$ excitations in Ar^{6+} are presented in Figs. 5 and 6. The forward-backward asymmetry parameter is defined by

$$A = \frac{\int_0^{\pi/2} \frac{d\sigma}{d\theta} \sin\theta d\theta - \int_{\pi/2}^{\pi} \frac{d\sigma}{d\theta} \sin\theta d\theta}{\int_0^{\pi} \frac{d\sigma}{d\theta} \sin\theta d\theta}, \quad (12)$$

where $d\sigma/d\theta$ is the differential cross section as a function of laboratory scattering angle θ . For $0 < A < 1$, forward scattering is largest; while for $-1 < A < 0$, backward scattering dominates. In Fig. 5 the excitation threshold energies are 17.6, 41.2, and 71.4 eV for the $3s \rightarrow 3p$, $3d$, and $4s$ transitions, respectively. The $3s \rightarrow 4s$ monopole transition in Ar^{7+} exhibits pronounced backward scattering to almost 2.5 times the threshold energy. In Fig. 6 the excitation threshold energies are 14.2 and 21.2 eV for the $3s^2 1S \rightarrow 3s3p^3 3P$ transition, respectively. The asymmetry parameter for the $3s^2 1S \rightarrow 3s3p^1 3P$ dipole transition in Ar^{6+} is quite similar to the one for the $3s \rightarrow 3p$ transition in Ar^{7+} over a wide energy range. The $3s^2 1S \rightarrow 3s3p^3 3P$ spin-forbidden transition in Ar^{6+} has a negative asymmetry parameter for energies up to 5.0 times the threshold energy. As pointed out before [22], the spin-forbidden angular distribution may be difficult to

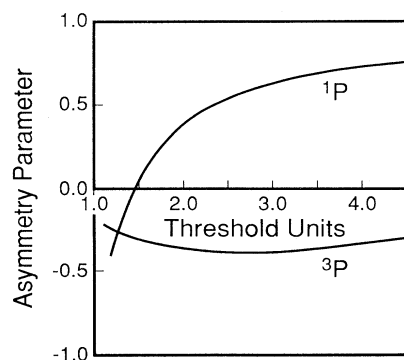


FIG. 6. The forward-backward asymmetry parameter for the $3s^2 1S \rightarrow 3s3p^3 3P$ excitations in Ar^{6+} . (Threshold unit is the incident energy divided by the excitation energy.)

observe experimentally; the resonant contribution to the cross section is relatively strong and will change the angular distribution significantly.

VI. SUMMARY

The quantal distorted-wave and classical-trajectory Monte Carlo methods are used to calculate electron-impact excitation cross sections for the $3s \rightarrow 3p$ dipole transition in Ar^{7+} . Upon comparison the classical calculations are able to reproduce the main features of the differential cross section with scattering angle, although not the detailed diffraction pattern. Further differential cross-section calculations, using the distorted-wave method, were carried out for the $3s \rightarrow 3p$, $3d$, and $4s$ transitions in Ar^{7+} and $3s^2\ ^1S \rightarrow 3s3p\ ^3,^1P$ transitions in Ar^{6+} in order to ascertain the degree of backward scattering

likely to be found for multiply charged ions. All transitions near the threshold for excitation were found to be dominated by backscattering. Excitation cross sections in the near-threshold energy region are further complicated by the presence of autoionizing resonance structures. Their inclusion within a nonperturbative close-coupling or perturbative distorted-wave approach will lead to resonance structure superimposed on the background results reported in Sec. V for the forward-backward asymmetry parameter.

ACKNOWLEDGMENTS

This work was supported by the U.S. Department of Energy under Contract No. DE-FG05-86ER53217 with Auburn University and Contract No. DE-AC05-85OR21400 with Martin Marietta Energy Systems, Inc., contract operator for Oak Ridge National Laboratory.

-
- [1] B. A. Huber, C. Ristori, P. A. Hervieux, M. Maurel, C. Guet, and H. J. Andra, *Phys. Rev. Lett.* **67**, 1407 (1991).
 - [2] E. K. Wahlin, J. S. Thompson, G. H. Dunn, R. A. Phaneuf, D. C. Gregory, and A. C. H. Smith, *Phys. Rev. Lett.* **66**, 157 (1991).
 - [3] S. J. Smith, K. F. Man, R. J. Mawhorter, I. D. Williams, and A. Chutjian, *Phys. Rev. Lett.* **67**, 30 (1991).
 - [4] N. F. Mott and H. S. W. Massey, *The Theory of Atomic Collisions* (Clarendon, Oxford, 1965).
 - [5] M. A. Hayes and M. J. Seaton, *J. Phys. B* **10**, L573 (1977).
 - [6] M. S. Pindzola, D. C. Griffin, and C. Bottcher, *Phys. Rev. A* **39**, 2385 (1989).
 - [7] R. Abrines and I. C. Percival, *Proc. Phys. Soc.* **88**, 81 (1966).
 - [8] D. C. Griffin and M. S. Pindzola, *Phys. Rev. A* **42**, 248 (1990).
 - [9] C. F. Fischer, *Comput. Phys. Commun.* **64**, 369 (1991).
 - [10] R. L. Kelly, ORNL Pub. No. 5922, 1982 (unpublished).
 - [11] D. R. Schultz, L. Meng, and R. E. Olson, *J. Phys. B* **25**, 4601 (1992).
 - [12] D. R. Schultz and C. O. Reinhold, *J. Phys. B* **23**, L9 (1990).
 - [13] R. E. Olson and T. J. Gay, *Phys. Rev. Lett.* **61**, 302 (1988).
 - [14] R. H. Garvey, C. H. Jackman, and A. E. S. Green, *Phys. Rev. A* **12**, 1144 (1975).
 - [15] R. L. Becker and A. D. MacKellar, *J. Phys. B* **17**, 3923 (1984).
 - [16] D. C. Griffin, M. S. Pindzola, and N. R. Badnell, in *Proceedings of the VI International Conference on the Physics of Highly Charged Ions*, edited by P. Richard, M. Stöckli, C. L. Cocke, and C. D. Lin (AIP, New York, 1993), p. 473.
 - [17] R. E. H. Clark, private communication.
 - [18] D. R. Schultz and R. E. Olson, *J. Phys. B* **24**, 3409 (1991).
 - [19] P. A. Hervieux and C. Guet, *Phys. Rev. A* **47**, 2031 (1993).
 - [20] C. O. Reinhold and J. Burgdorfer, *J. Phys. B* **26**, 3101 (1993).
 - [21] I. C. Percival and D. Richards, *Adv. At. Mol. Phys.* **11**, 1 (1975).
 - [22] D. C. Griffin, M. S. Pindzola, and N. R. Badnell, *Phys. Rev. A* **47**, 2871 (1993).